Int J Thermophys (2015) 36:2356–2369
DOI 10.1007/s10765-015-1926-z

Comparative Analysis of Thermography Studies and Electrical Measurement of Partial Discharges in Underground Power Cables

A. Gonzalez-Parada[1] · R. Guzman-Cabrera[1] · M. Torres-Cisneros[1] · J. R. Guzman-Sepulveda[2]

Received: 28 October 2014 / Accepted: 23 June 2015 / Published online: 3 July 2015

Abstract The principal cause of damage in underground power cable installations is partial discharge (PD) activity. PD is a localized non-linear phenomenon of electrical breakdown that occurs in the insulating medium sitting between two conducting materials, which are at different potentials. The damage to the insulating material is induced by the AC voltage to which the insulator is subjected during the discharge process, and it can be directly or indirectly measured by the charge displacement across the insulation and the cavity defect. Non-invasive detection techniques that help in identifying the onset of the discharge process are required as PD is a major issue in terms of maintenance and performance of underground power installations. The main locations of failure are the accessories at points of connection such as terminals or splices. In this article, a study of electrical detection of PD and image processing of thermal pictures is presented. The study was carried out by controllably inducing specific failures in the accessories of the installation. The temporal evolution of the PD signals was supported with thermal images taken during the test in order to compare the PD activity and thermal increase due to failure. The analysis of thermographic images allows location of the failure by means of intensity-based texture segmentation algorithms. This novel technique was found to be suitable for non-invasive detection of the PD activity in underground power cable accessories.

Keywords Failure onset · Partial discharges · Power cables · Texture segmentation · Thermography

✉ A. Gonzalez-Parada
gonzaleza@ugto.mx

[1] Engineering Division, University of Guanajuato, Km 3.5 + 1.8, Carr. Salamanca-Valle de Santiago, Com. de Palo Blanco, C.P. 36885 Salamanca, Guanajuato, Mexico

[2] CREOL, The College of Optics and Photonics, University of Central Florida, 4304 Scorpius St., Orlando, FL 32816-2700, USA

Nomenclature

C_a	Insulation without defect
C_b	Dielectric in series with the gaseous capacitance c
C_c	Cavity or part of the surface in which the PD occurs
A	Capacitor area
d	Insulation thickness
ε_0	Permittivity of free space
ε_r	Relative permittivity of the defect
t	Defect thickness
q	External charge displacement
q_1	Real charge displacement
V	Voltage in dielectric
V_i	Instantaneous PD inception voltage of the cavity
U	Voltage across the cavity before a discharge of c
ΔV	Drop voltage over c caused by the discharge
$E(\Omega_k)$	Local entropy in the neighborhood Ω_k
L	Maximal gray scale
$M_k \times N_k$	Window size
n_i	Pixel number with gray scale i in the neighborhood
P_i	Probability of gray scale i that appears in the neighborhood Ω_k

1 Introduction

The reliability and availability of a medium voltage under a ground power network are determined from the condition of all components in that grid. On underground power cable installations, the main points of failure are the accessories installed for making several connections between different grid components. Statistical percents of failure for cable installation are 52 % for splices, 43 % for terminals, 4 % for cable insulation, and 1 % for other events that are independent of the cable installation. Due to the fact that more than half of the breakdowns in the cable network are caused by internal faults in the insulation systems or accessories of the cable network, the diagnostics of new installations and service aged distribution power cables are very important to prevent such breakdowns and get knowledge about the actual condition of installations. By knowing the condition of the cable, early action can be taken before breakdown could occur during operation [1,2].

During aging of a defect in an underground power cable, different partial discharge (PD) mechanisms can occur. Aged defects generally have a lower inception voltage than small defects. PDs are measured by charge displacement in the cable caused by the defect; this is related to the energy dissipated during a discharge and the volume of the cavity [3]. Several systems designed by different manufacturers to measure the PD are available in the market; the technical difference between these systems is basically in the difference of the energizing source, the different sensors used, local determination, and whether measured according to IEC 60270 or charge determination [4,5].

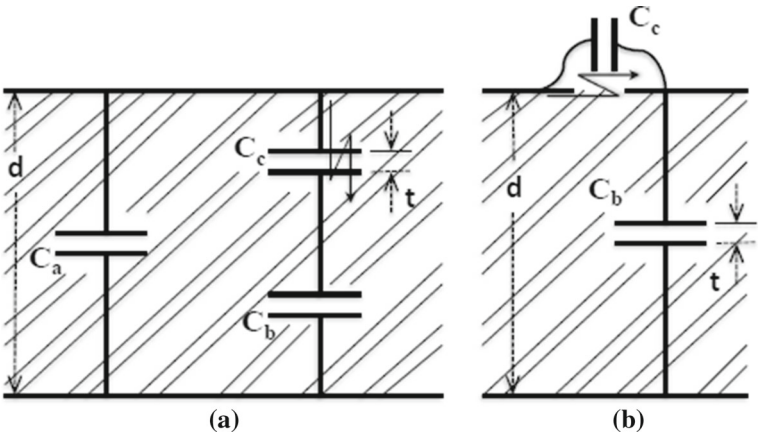

Fig. 1 Electrical representation of (a) internal partial discharges and (b) superficial partial discharges

In this article, a novel approach for detecting the PD is presented. The approach consists of comparing the measurement of electrical signals with the analysis and processing of thermographic images taken during the discharge process so that the PD activity through the simultaneous evaluation of electrical and thermal effects can be identified. The image processing applied to the thermographic pictures consists mainly of intensity-based texture segmentation algorithms that allow location of the failure. This approach allows for operating a scheme of non-invasive incipient failure detection since the onset of PD is successfully identified without temporarily shutting down the system for evaluation [5].

2 Theoretical Background

2.1 Partial Discharge Process

The definition of PD according to IEC 60270 is as follows: *Localized electrical discharge that only partially bridges the insulation between conductors and which is an electrical discharge that only partially bridges the insulation between conductors and which can or cannot occur adjacent to a conductor.*

PD is in general a consequence of the local electric stress concentrations in the insulation or the surface of the insulation. Generally, it appears as a pulse, having a duration of much less than 1 μs and is usually accompanied by emission of sound, light, heat, and chemical reactions. Considering that PDs are related to aging of the cable or bad accessories installed in a cable, charge measurements of a PD are useful. The PD type depends on the defective localization, and it could be either internal or on the surface. Figure 1 shows the electrical model for (a) a PD on internal defect insulation and (b) a PD on the insulation surface [6].

Considering the gas-filled cavity breakdown stress E_c, and treating the cavity as a series capacitance with the dielectric without a cavity in the dielectric (see Fig. 2) [7],

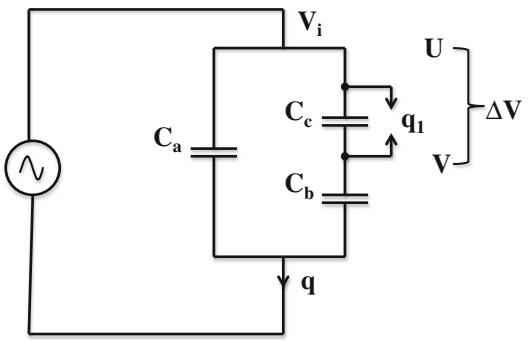

Fig. 2 PD electrical model

the capacitance can be written as

$$C_b = \frac{\varepsilon_0 \varepsilon_r A}{d - t} \tag{1}$$

$$C_c = \frac{\varepsilon_0 A}{t} \tag{2}$$

The voltage across the cavity is

$$U = \frac{C_b}{C_c + C_b} \Delta V = \frac{\Delta V}{1 + \frac{1}{\varepsilon_r}\left(\frac{d}{t} - 1\right)} \tag{3}$$

Accordingly, the voltage across the dielectric sufficient to initiate the discharge process in the cavity is

$$V_i = E_c \left[1 + \frac{1}{\varepsilon_r}\left(\frac{d}{t} - 1\right)\right] \tag{4}$$

When a PD occurs, some charge is displaced from C_c to C_b, as follows: the voltage across C_c drops to ΔV; since the voltage across C_b increases with ΔV, then the voltage over C_c becomes V, and the charge displacement in relation to C_b is given by $q = C_b \Delta V$.

The energy dissipated during a discharge can be related to the charge accordingly as follows; before discharge, the energy stored in C_c is

$$W_{C_c} = \frac{1}{2} C_c U^2 \tag{5}$$

after discharge, the energy stored in C_c is

$$W_{C_c} = \frac{1}{2} C_c V^2 \tag{6}$$

The total dissipated energy in the cavity becomes

$$W_t = \frac{1}{2} C_c \left(U^2 - V^2\right) = \frac{1}{2} C_c \Delta V \left(U + V\right). \tag{7}$$

Usually $C_b << C_c$, then the dissipated energy becomes

$$W_t \approx \frac{1}{2} C_b \Delta V \cdot V_{\mathrm{i}} = \frac{1}{2} q V_{\mathrm{i}}. \tag{8}$$

This energy is dissipated as heat, and can be detected at the moment prior to failure by an IR camera. In the case of an incipient failure, the energy released is not sufficiently large so that the temperature rise cannot be detected by a thermal imaging camera. Therefore, variations in the texture of the image could be detected by means of a digital processing of thermal images.

2.2 Image Process Methodology

The proposed technique is based on feature extraction through texture analysis for the identification and discrimination of suspicious areas related to the failure. As texture-based analytical methods characterize texture in terms of the extracted feature, segmentation depends not only on the images under study but also on the aim for which the image texture is used [8]. General definitions of the image processing can be seen in Appendix 1 at the end of this article [9–11].

A general flow diagram of the proposed image processing is shown in Fig. 3. In general, the process begins with an input thermal image that has to be processed in different stages until an output image containing the regions of interest, and thus the possible system failures, is generated.

The main stages of the process are the preprocessing of the input image, the identification of the background and object textures, and the segmentation and extraction of the regions of interest. However, since the preprocessing stage (i.e., image sharpen-

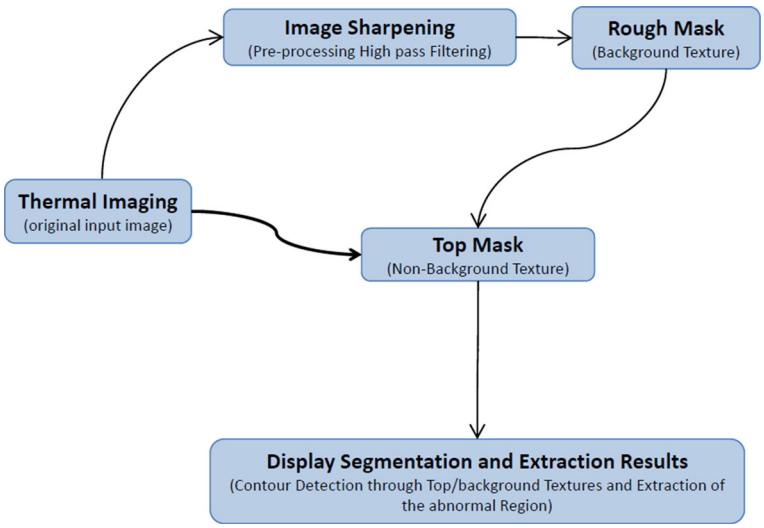

Fig. 3 Flow diagram of the intensity-based texture segmentation algorithm

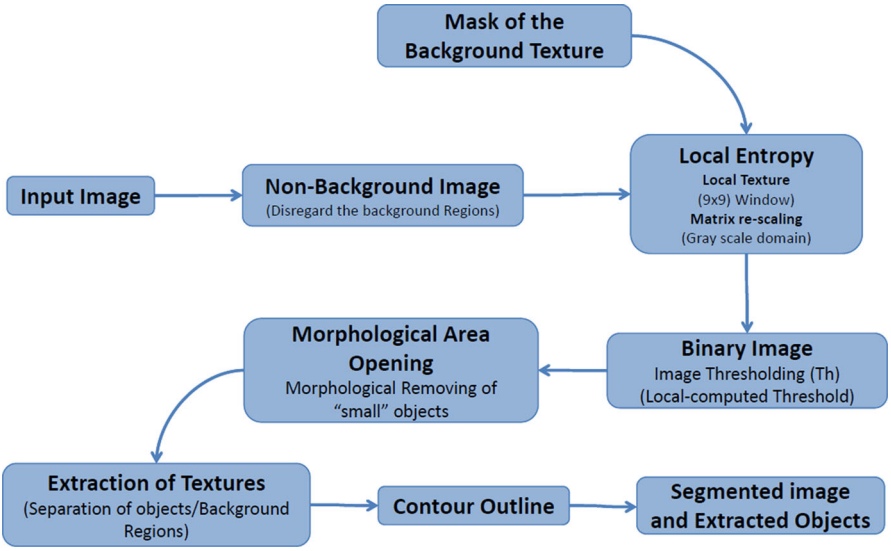

Fig. 4 Internal structure of the stage where the object's texture is extracted

ing) serves only to enhance the fine details of the input image, the segmentation and extraction stages become more transcendental.

As shown in Fig. 3, the regions of interest are identified and then extracted using the background texture as a contrast mask against the original input image. This means that the regions identified as part of the object texture are defined directly by the background regions in the rough mask. A more detailed view of the segmentation and extraction stages, which are the critical steps in our approach, is shown in Fig. 4.

Despite a wide variety of segmentation algorithms can be found in the literature, it is more natural to choose entropy-based rather than gradient-based texture segmentation algorithms due to the well- acknowledged superior performance in the case of targets with fuzzy, unclear boundaries and in which the transition regions are not well defined [12].

Accordingly, the entropy of the image is calculated through local statistical measurements of randomness by means of a small region Ω_k of size $(M_k \times N_k)$ that operates as a running window over the entire image such that the entropy within this small region is calculated in the following way [13]:

$$E(\Omega_k) = -\sum_{i=0}^{L-1} P_i \log(P_i), \tag{9}$$

where

$$P_i = \frac{n_i}{(M_k \times N_k)}. \tag{10}$$

Although the images were not processed *in situ* and the computational resources allow for more sophisticated processing, the proposed algorithm considers only the first-

order entropy in order to minimize the computational cost in future in-line processing applications, even though it is well known that additional structural information of the image can be accessed from higher-level calculations [14].

The calculation of the local entropy described above is the initial step in the definition of the so-called background texture, as shown in Fig. 4. In this particular case, the calculation of the local entropy is performed over a preprocessed image, sharpened by using standard high-pass filtering techniques. The local entropy was calculated using a window size of 9×9 pixels, i.e., $M_k = N_k = 9$, and the output of this stage, an image containing the local entropy, was then binarized by simple thresholding (Th) using the reference value shown in Fig. 4.

The binarized image is a primitive version of the background texture. However, additional treatment of this image is needed in order to obtain better performance. In this particular case, first removing the "small" objects and then smoothing the edges of the regions previously binarized clean this image. Removing the "small" objects was performed by using the "area opening" method, while the edge smoothing was carried out by the standard sequential process of dilation followed by erosion, using a mask size of 9×9 pixels in both cases.

The identification of the so-called object texture is now possible since the binary image containing the background texture allows for a direct separation of the "non-background" regions. A new image is obtained by extracting only the non-background regions of the original image.

The local entropy is calculated over this new image in a similar manner to the first calculation. Unlike the first calculation, which is performed over the full original image, this time the image contains a combination of pixels with the original values and black pixels corresponding to the background texture. This allows recalculating the local entropy only over regions of interest with the certainty that the regions identified as part of the background texture do not contribute to it, since the entropy is minimal for regions consisting of pixels with the same gray value [15]. After thresholding the resulting image, a binary, preliminary version of the object texture is available.

This preliminary version of the object texture was cleaned up in similar fashion to the background texture, i.e., removing small objects and edge smoothing. The final, binary image contains the regions of interest that are to be extracted from the original image.

More details in the specific parameters used in each stage of the process can be found elsewhere [16]

2.3 Experimental Technique

In order to validate this image analysis process, a laboratory test was performed considering the induced failure in terminals. A photograph of the experimental test setup is illustrated in Fig. 5. A power transformer is used to simulate the high voltage applied in the transmission line, and the charge is induced in the line by a current transformer. Commercial 1/0 AWG cables with 100 % XLP insulation and wire screen were used in the experiments.

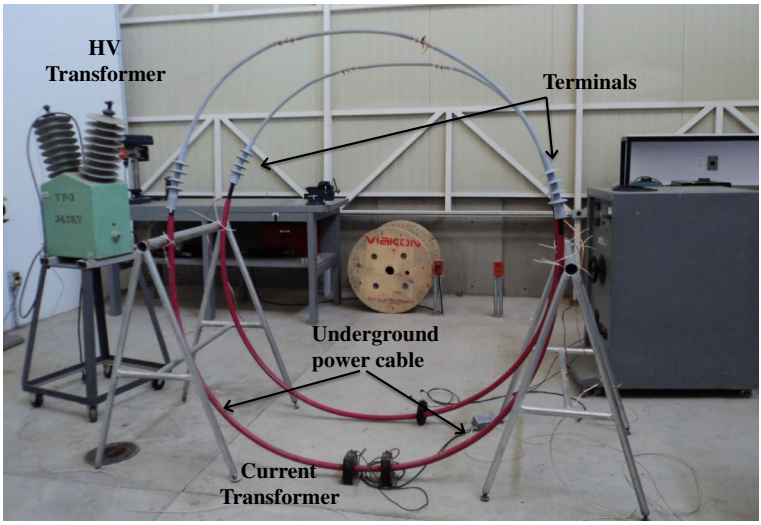

Fig. 5 General test setup for electrical PD detection in underground power cable model

The voltage between the phase and ground terminals is set to 15 kV, and suitable silicon terminals were used (Elastimold model PCT1 silicon terminals for 1/0 AWG power cables). Under these conditions, a current of 60 A circulates in the system considering a real charge of the line.

A failure is induced in the terminal having a small separation of the terminal stress cone and the outer semiconductive layer. This separation induces a superficial PD in the terminal causing a temperature increment by the charge transference and electrical activity. As shown in current circulating in the cable, Fig. 6 shows a picture of the failure induced in the terminal where the separation stress cone of the terminal and the cable's outer semiconductive layer can be clearly appreciated.

In order to measure the changes in the electrical signals as the failure occurs, the system was instrumented with a lab-made Rogowski coil, as shown in Fig. 7. The coil is connected to a standard digital oscilloscope (Fluke 190-102) such that the electrical current circulating through the part of the system affected by the induced failure was continuously monitored. This instrumentation allows identifying the PD activity and ensuring the occurrence of the failure.

Indeed, PD activity was verified in both terminals by means of the sensors shown in Fig. 7. The signal obtained was plotted to see the difference between the terminal with a defect and the terminal without failure. Figure 8 shows the PD present in the terminal with failure, the absence being noticed in the terminal in good condition.

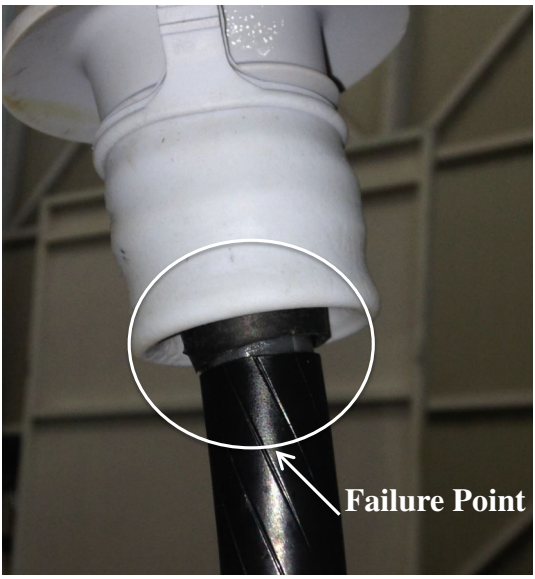

Fig. 6 Terminal with failure induced in the cable with the stress cone separated from the outer semiconductive screen

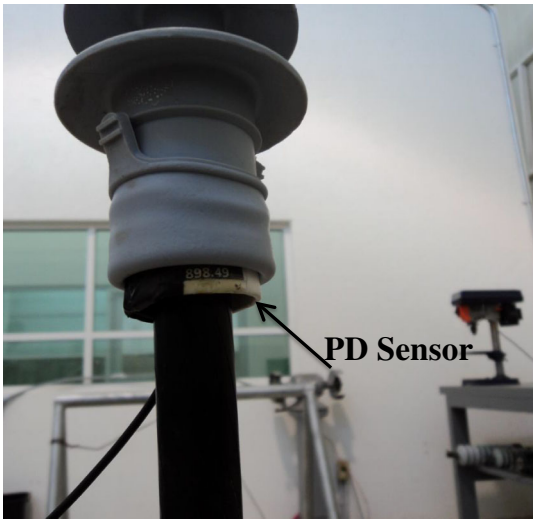

Fig. 7 Position of the sensor in the terminal to check the PD activity in cable

3 Results

Figures 9 and 10 show pictures of the terminals with failure and without failure; these pictures were taken with the thermography camera Fluke Ti 132 under infrared palettes and white light, respectively. The temperature scale shown in the infrared image is the actual temperature measured using the camera calibration such that the temperature distribution over the pictures is also provided.

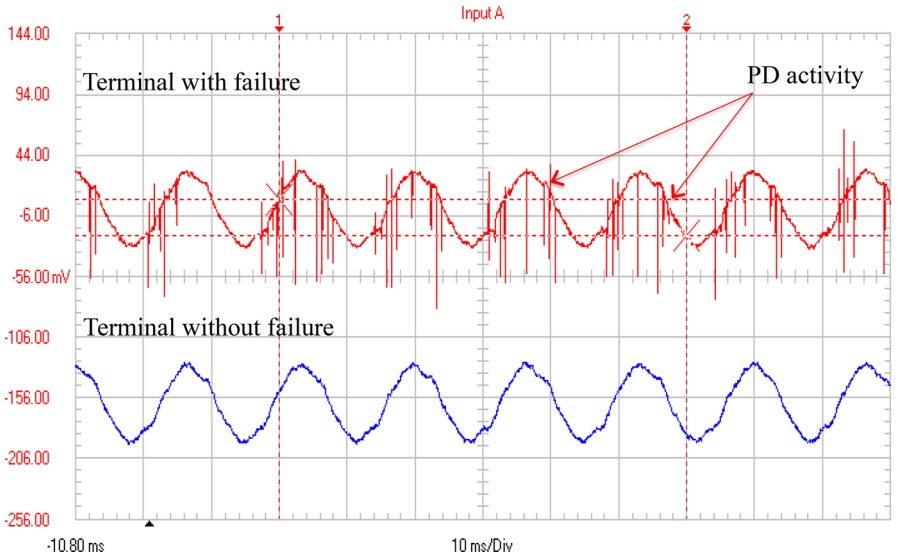

Fig. 8 PD signal activity obtained from terminal with failure (*upper*) and terminal in good condition (*lower*)

Fig. 9 Pictures of the terminal with failure and partial discharges in two different color palettes: (a) white light and (b) infrared

Despite this, an accurate contactless temperature measurement can be achieved with a good calibration of the infrared camera, the proposed image processing never sees this calibration but only the textures defined by the gray levels that naturally arise due to thermal effects.

In order to orientate the analysis of the thermal effects to the region of interest, infrared images of the experimental setup were processed digitally by using segmentation and extraction algorithms based on the texture and morphological image analyses described above.

Figures 11 and 12 show the results of a processed picture of the experimental setup after segmentation and extraction, respectively. It can be clearly seen that the region of the point of failure can be successfully identified. The proposed instrumentation

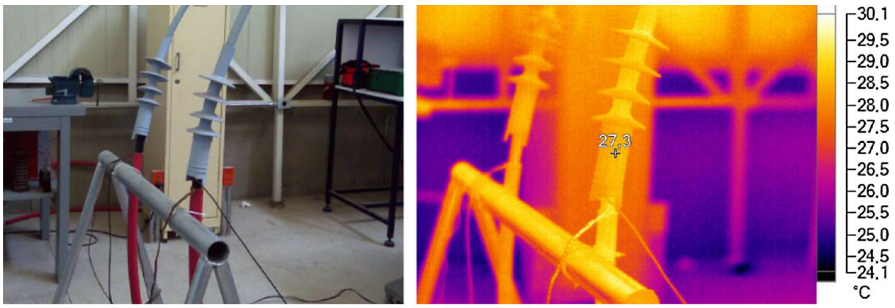

Fig. 10 Pictures of the terminal in good condition in two different color palettes: (a) white light and (b) infrared

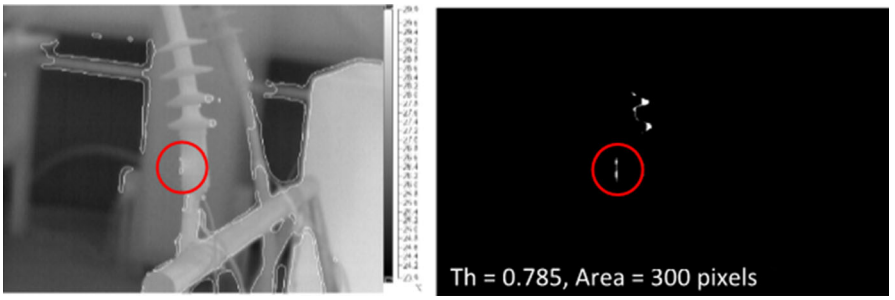

Fig. 11 Segmentation and extraction of the point of failure in terminal with failure

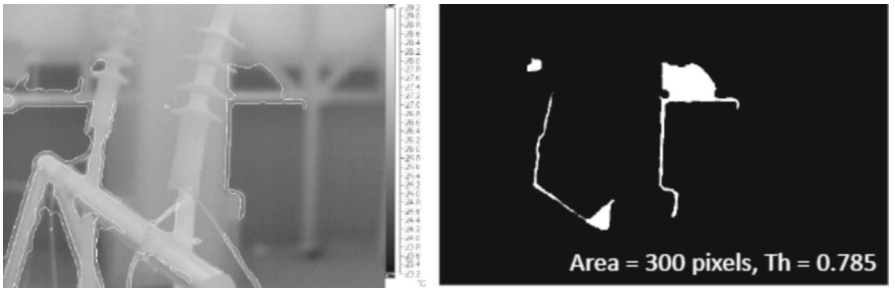

Fig. 12 Segmentation and extraction of the terminal in good condition without failure point

not only allows calibrated measures of the temperature over several regions of the experimental setup but also validates the physical location of the failure obtained from the imaging process.

Moreover, since the digital processing is to operate on infrared images obtained from contactless instrumentation, the proposed approach provides a suitable and powerful tool for safe, continuous, and effective failure detection that allows remote control and uninterrupted *in situ* measurement in which a disconnection line is not required.

4 Conclusions

The proposed monitoring method and analysis system test setup allow inducing a variety of controlled failures in order to accurately compare the electrical behavior of the partial discharges phenomenon with thermal images. This detailed characterization can help diagnose and prevent a variety of failures in further applications.

The location where the induced failure occurs is confirmed by the processing of infrared images based on texture segmentation and morphological extraction algorithms thus allowing related changes in the electrical behavior caused by the induced failure, resulting in reliable performance of the proposed measurement and analysis system.

Acknowledgments This work was supported in part by the University of Guanajuato by Grant PIFI 2013.

Appendix 1: Image Processing Definitions Textual Citation from References [9–11]

Region of Interest (ROI) is a region of interest (often abbreviated ROI), is a selected subset of samples within a dataset identified for a particular purpose. An image may be considered to contain sub-images sometimes referred to as regions of interest, ROIs, or simply regions.

Texture is concerned with the spatial distribution of the image intensities and discrete tonal features. When a small area of the image has little variation of discrete tonal features, the dominant property of that area is gray tone. When a small area has wide variation of discrete tonal features, the dominant property of that area is texture. There are three things crucial in this distinction: (1) the size of the small areas, (2) the relative sizes of the discrete tonal features, and (3) the number of distinguishable discrete tonal features. Texture can be described along dimensions of uniformity, density, coarseness, roughness regularity, intensity, and directionality.

Image segmentation is a process which typically partitions the spatial domain of an image into mutually exclusive subsets, called regions, each one of which is uniform and homogeneous with respect to some property such as tone or texture and whose property value differs in some significant way from the property value of each neighboring region. Regions produced by an image segmentation process using image intensity as a property value produce regions which are called discrete tonal features.

Preprocessing is an operation applied before pattern identification is performed. Preprocessing produces, for the categories of interest, pattern features which tend to be invariant under changes such as translation, rotation, scale, illumination level, and noise. In essence, preprocessing converts the measurement patterns to a form which allows a simplification in the decision rule. Preprocessing can bring into registration, bring into congruence, remove noise, enhance images, segment target patterns, detect, center, and normalize objects of interest.

Image processing or picture processing encompasses all the various operations which can be applied to image data. These include, but are not limited to, image compression, image restoration, image enhancement, preprocessing, quantization, spatial filtering, matching, and recognition techniques.

Background Texture It is the bottom part of the image. This structure is compared and it decides, based on a threshold, the part that must be removed.

Feature extraction is the process by which an initial measurement pattern or some subset of measurement patterns is transformed to a new pattern feature. Sometimes feature extraction is called property extraction. The word pattern can be used in three distinct senses: (1) as measurement pattern; (2) as feature pattern; and (3) as the dependency pattern or patterns of relationships among the components of any measurement n-tuple or feature n-tuple derived from units of a particular category and which are unique to those n-tuples, that is, they are dependencies which do not occur in any other category.

The ***contrast of an object against its background*** can be measured by (1) its contrast ratio, which is the ratio between the higher of object transmittance or background transmittance and the lower of object transmittance or background transmittance; (2) its contrast difference, which is the difference between the higher density of object or background and the lower density of object or background; (3) its contrast modulation, which is the difference between the darker of object or background image intensity and the lighter of the two divided by the sum of object image intensity and background image intensity.

Mathematical morphology refers to an area of image processing concerned with the analysis of shape. The basic morphologic operations consist of dilating, eroding, opening, and closing an image with a structuring element.

Dilating an image I by a structuring element s having support or domain S produces a dilated image denoted by $I \oplus S$ which is defined by $I \oplus S\,(r, c) = max_{(i,j)\in S}\{I\,(r-i, c-j) + S\,(i,\, j)\}$. Dilating is a commutative, associative, translation invariant, and increasing operation. Dilating is the dual operation to eroding.

Eroding an image I by a structuring element s having support or domain S produces an eroded image denoted by $\boldsymbol{I \ominus S}$ which is defined by $\boldsymbol{I \ominus S\,(r, c) = min_{(i,j)\in S}\{I\,(r+i, c+j) + S\,(i, j)\}}$. Eroding is a translation invariant and increasing operation. It is the dual operation to dilating.

Opening an image I with a structuring element s produces an opened image denoted by $I \circledcirc S$ which is defined by $I \circledcirc S = (I \ominus S) \oplus S$. Opening is an increasing, antiextensive, and idempotent operation. It is the dual operation to closing. Opening an image with a disk-shaped structuring element smooths the contour, breaks narrow isthmuses, and eliminates islands and capes smaller in size or width than the disk structuring element.

References

1. E. Gulski, E. Lemke, M. Gamlin, E. Gockenbach, W. Hauschild, E. Pultrum, Electra **35**, 43 (2003)
2. G. Paoletti, A. Golubev, presented at IEEE IAS Pulp Pap. Ind. Conf. (2009)
3. M. Tozzi, Ph.D Thesis, University of Bologna (2010)
4. E. Lemke, S. Berlijn, E. Gulski, M. Muhr, E. Pultrum, T. Strehl, W. Hauschild, J. Rickmann, G. Rizzi, Electra **61**, 241 (2008)
5. E. Lemke, E. Gulski, W. Hauschild, R. Malewski, P. Mohaupt, M. Muhr, J. Rickmann, T. Strehl, F.J. Wester, Electra **63**, 226 (2006)
6. R. Bartnikas, IEEE Trans. Electr. Insul. **25**, 1 (1990)

7. R. Bartnikas, IEEE Trans. Electr. Insul. **9**, 5 (2002)
8. H.D. Cheng, X. Cai, X. Chen, L. Hu, X. Lou, Patterrn Recognit. **36**, 2967 (2003)
9. I.T. Young, J.J. Gerbrands, L.J. Van Vliet, *Fundamentals of Image Processing* (Delft University of Technology, Delft, The Netherlands, 1998)
10. R.M. Haralick, L.G. Shapiro, Pattern Recognit. **24**, 69 (1991)
11. R.M. Haralick, L.G. Shapiro, *Glossary of Computer Vision Terms. Optical Engineering* (Marcel Dekker Incorporated, New York, 1994), p. 42
12. R.C. Gonzalez, R.E. Woods, S.L. Eddins, *Digital Image Processing Using MATLAB*, chap. 11 (Pearson Prentice Hall, Upper Saddle River, NJ, 2003)
13. T. Pun, Signal Process. **2**, 223 (1980)
14. J.J. Gerbrands, Ph.D. Thesis, Delft University of Technology (1998)
15. J. Yáñez, S. Muñoz, J. Montero, Graph coloring inconsistencies in image segmentation. Comput. Eng. Inf. Sci. **1**, 435 (2008)
16. R. Guzmán-Cabrera, J.R. Guzmán-Sepúlveda, M. Torres-Cisneros, D.A. May-Arrioja, J. Ruiz-Pinales, O.G. Ibarra-Manzano, G. Aviña-Cervantes, A. González Parada, Int. J. Thermophys. **34**, 1519 (2013)